Scientific Research Publishing

Advances in Materials Physics and Chemistry, 2026, 16(6), 249-262
https://www.scirp.org/journal/ampc
ISSN Online: 2162-5328
ISSN Print: 2162-531X

Characterization of a Clay Raw Material from Oualle: Uses in Ceramics

Bobet Ouanmini[1], Ganon François[2], Bamogo Halidou[3], Seynou Mohamed[4], Zerbo Lamine[4], Gilles Escadeillas[5]

[1]Ecole Normale Supérieure, Bongor, Tchad
[2]Ecole Normale Supérieure, Ndjaména, Tchad
[3]Laboratoire de Chimie et Energies Renouvelables, Université Nazi Boni, Bobo-Dioulasso, Burkina Faso
[4]Université Joseph Ki-Zerbo, Ouagadougou, Burkina Faso
[5]Laboratoire Matériaux et Durabilité des Constructions (LMDC), Université de Toulouse, INSA, Toulouse, France
Email: bobetouanmini97@gmail.com

How to cite this paper: Ouanmini, B., François, G., Halidou, B., Mohamed, S., Lamine, Z. and Escadeillas, G. (2026) Characterization of a Clay Raw Material from Oualle: Uses in Ceramics. *Advances in Materials Physics and Chemistry*, **16**, 249-262.
https://doi.org/10.4236/ampc.2026.166013

Received: April 15, 2026
Accepted: June 5, 2026
Published: June 8, 2026

Abstract

This paper evaluates Ouallé clay for ceramic applications using geotechnical, chemical, mineralogical, thermal, and firing-based characterization methods. The study finds that the clay is mainly kaolinite-rich, moderately plastic, and potentially suitable as a base material for faience and fired clay products. The fired specimens show acceptable shrinkage, but the porosity remains high and the maximum compressive strength is moderate.

Keywords

Clay, Ceramics, Tiles

1. Introduction

Clay has been used for pottery for a very long time, and still is today in many countries around the world for building houses. It is the raw material for making tiles and bricks. The importance of clay-based materials in the ceramics industry stems from their plasticity and the ability of the shaped product to retain its form after firing.

This work is part of a project to characterize and develop the potential of clay sites in Burkina Faso.

Indeed, we are interested here in developing a local clay raw material for use in ceramics. This will involve the physicochemical characterization of the clay from Ouallé and technological tests for its potential use in ceramic tiles.

2. Characterization of Raw Materials

2.1. Site Presentation

The site is located at 12˚54 North Latitude and 2˚20 West Longitude in Burkina Faso (Figure 1). It is frequently used by the local population for building houses and/or for manufacturing objects.

For this study, several techniques were used to characterize this clay.

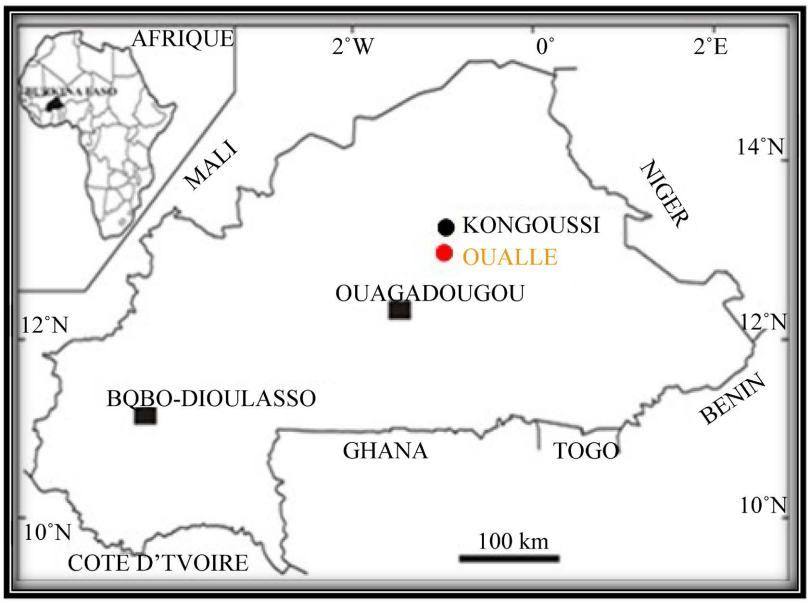

Figure 1. Map of Burkina Faso. locating Ouallé.

2.2. Geotechnical Characterization

2.2.1. Humidity Level (HL)

Heating a quantity of the sample previously air-dried to 105˚C within 24 hours.

The results of the various moisture content tests are recorded in Table 1. The average moisture content of our sample is 0.23%. This value indicates that the sample is only slightly hydrated by atmospheric water. This results in a low presence of swelling minerals in our raw material.

Table 1. Humidity levels.

Trials	m_1 (g)	m_2 (g)	$(m_1 - m_2)$ (g)	H. L (%)
1	6.964	6.949	0.015	0.211
2	6.754	6.738	0.016	0.242
3	7.443	7.425	0.018	0.243
	Average value of H. L			0.232

m_1: mass of the sample before drying; m_2: mass of the sample after drying at 105˚C for 24 hours.

2.2.2. Loss on Fire (LF)

The loss on ignition at 1000˚C was determined using a NABERTHERM C250 fur-

nace for 2 hours. The results are shown in Table 2. The average loss on ignition of the sample, 10.58%, is quite significant and indicates a predominance of clay minerals in our sample. This loss corresponds to the dehydroxylation of the clay minerals, particularly illite and kaolinite, which are sensitive to the temperature range used.

Table 2. The loss to fire of the Ouallé clay.

Trials	m_2 (g)	m_3 (g)	$(m_2 - m_3)$ (g)	L. F (%)
1	6.949	6.213	0.736	10.590
2	6.738	6.007	0.731	10.842
3	7.425	6.660	0.765	10.302
	Average value of L. F			10,578

m_2: mass of clay material steamed at 105˚C; m_3: mass of clay material after baking at 1000˚C for 2 hours in a kiln.

2.2.3. Particle Size

We used the laser diffraction method. The device used is a Malverne 2000 type laser particle size analyzer. It consists of a He-Ne laser source which emits a monochromatic wave of a very precise wavelength, a measuring cell and a data acquisition system.

Particle size analysis was performed on the fraction smaller than 200 µm. The volumetric curve (Figure 2) of the Ouallé clay indicates that it is composed of three population types centered at 0.6 µm, 15 µm, and 190 µm, corresponding respectively to the clay fraction, the silty fraction, and the sandy fraction [1].

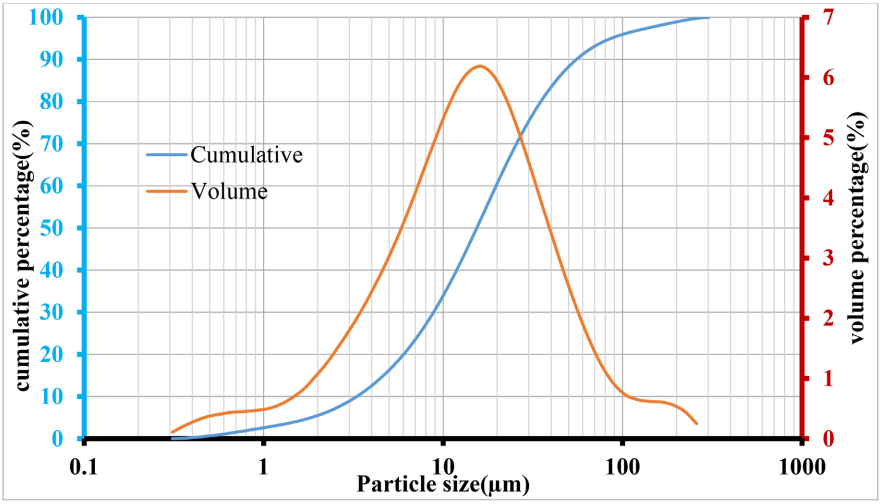

Figure 2. Volumetric and cumulative particle size distribution curves of the Ouallé clay.

The cumulative particle size distribution curve allows for the determination of d_{10}, d_{50}, and d_{90} values (Table 3). These results show that 50% of the Ouallé particles have a diameter of 14.22 µm. The d10 is close to 2 µm, indicating that the clay

fraction is approximately 10%. The d_{50} and d_{90} values show that the majority of the grains in the Ouallé clay therefore belong to the silty and sandy families [2].

Table 3. Particle size parameters of the Ouallé clay.

	d_{10}	d_{50}	d_{90}
Sample (μm)	3.09	14.22	56.23

2.2.4. Atterberg Limits

The results of the tests conducted on the sample are presented in **Table 4**. According to numerous studies, the plasticity of clays depends on the nature of their clay minerals and is inversely proportional to grain size. Clays with a large particle size distribution generally exhibit low plasticity. Indeed, the specific surface area of large particles reduces the amount of water adsorbed, which leads to a decrease in plasticity [3].

The plasticity index of our sample is approximately 10.53%. According to **Table 5**, the clay studied falls into the category of moderately plastic clays. This plasticity may be related to the presence of minerals such as illite and kaolinite, but is also limited by the presence of quartz.

Table 4. Atterberg limits of the Ouallé clay.

Sample	Liquidity limit (%)	Limit of plasticity (%)	Plasticity index (%)
Ouallé	33.1	22.6	10.5

Table 5. Soil classification based on their plasticity index [4].

Plasticity index	Degree of plasticity
$0 < I_p < 5$	Non-plastic (the test loses its meaning in this range of values)
$5 < I_p < 15$	Moderately plastic
$15 < I_p < 40$	Plastic
$I_p > 40$	Very plastic

2.2.5. Microstructure

The morphology of the clay platelets studied was observed using scanning electron microscopy (SEM). The instrument used was a Hitachi S-2500 microscope operating at 20 kV. Before observation, the samples (clay fraction) were placed in solution in double-distilled water. The agglomerates were separated by ultrasonic stirring for 20 minutes. The suspension is then deposited on a support, dried and metallized with a layer (Au/Pd).

Figure 3 shows the SEM image of the Ouallé clay. The image reveals a layered structure characteristic of the presence of a large quantity of clay minerals such as kaolinite. This significant clay phase content indicates that the results of the particle size analysis do not reflect reality. This is due to the layered nature of the

particles, which are far from being the spheres on which laser diffraction theory is based.

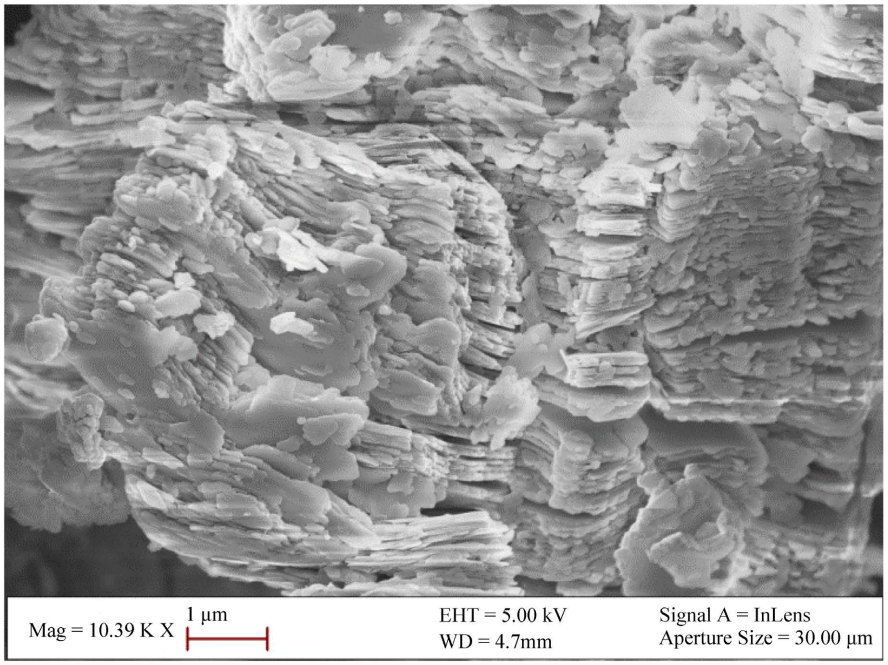

Figure 3. SEM image of Ouallé.

2.3. Elemental Chemical Analysis

The compounds are solubilized at 1250˚C with lithium tetraborate ($LiBO_4$) before forming beads which are then used for analysis.

The results of the elemental chemical analysis of the Ouallé clay are recorded in Table 6.

This table shows that our clay is a silico-aluminate. A moderate iron oxide content (4.41%) is also noted, due to the presence of goethite. The K_2O content (1.04%) indicates that this clay likely contains illite.

Table 6. Elemental chemical analysis of Ouallé.

Oxides	SiO_2	Al_2O_3	Na_2O	K_2O	CaO	MgO	Fe_2O_3	TiO_2	LF	total
%	53.21	29.18	-	1.3	0.17	0.32	4.51	0.68	10.58	100

Table 7. The major oxides and their characteristics.

	SiO_2	Al_2O_3	$Fe_2O_3 + TiO_2$	$K_2O + MgO + CaO$
Rate (%)	53.21	29.18	5.19	1.79
characters	degreaser	refractory	dye	fondant

Based on these results, we can deduce that the clay studied is silica (SiO_2 content between 41.5% and 56.4%) and not refractory, since refractory clays have an Al_2O_3

content greater than 45%. It will not fire white, as a clay that fires white is characterized by an Fe_2O_3 content always less than 1.5% [5]. The high flux content (K_2O, MgO, and CaO) improves the technological properties of the ceramic material. Ouallé clay is a good mixture of plasticizer, flux, degreaser, and colorant. Given the varying levels of the major oxides (Table 7), it can be said that Ouallé clay can be used in the manufacture of ceramic tiles and fired bricks.

2.4. Mineralogical Characterization

2.4.1. X-Ray Diffraction (XRD)

The instrument used was a Philips PW 1729 diffractometer operating at 40 kV with a current of 40 mA. The radiation used was CuK*α*. EVA and CRISTAL software were used for diffractogram processing.

The analysis of the X-ray diffraction spectrum (Figure 4) was carried out using ASTM data sheets. The Ouallé clay is composed primarily of kaolinite, goethite, quartz, and illite. Illite and kaolinite act as plasticizers, quartz ensures the mechanical strength of the raw clay, and goethite gives the tiles their color after firing.

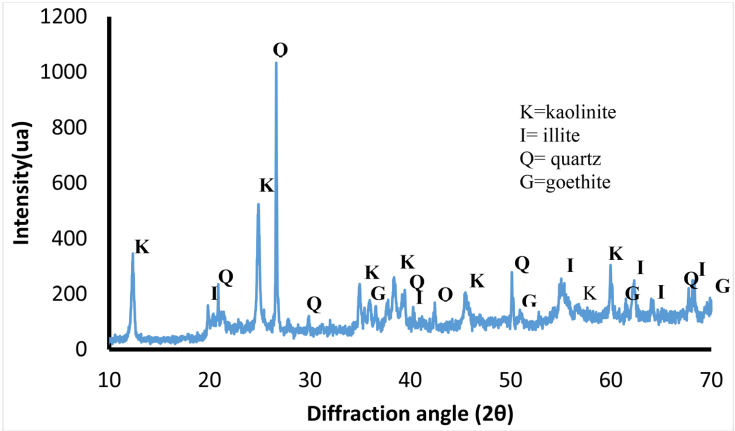

Figure 4. Diffractogram of the Ouallé clay.

2.4.2. Infrared (IR) Spectrometry

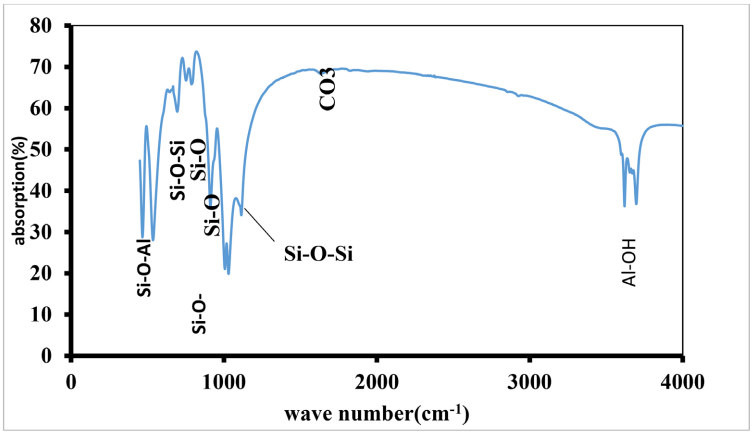

Figure 5. Infrared spectrum of Ouallé clay.

Infrared spectra were recorded using a PERKIN ELMER Spectrum One IR spectrophotometer. One-cm diameter pellets were prepared for each sample (5 mg) using KBr (300 mg) as a matrix. The wavelength range explored was 400 to 4000 cm^{-1}.

Examination of the infrared spectrum in **Figure 5** shows that:

The bands at 463, 532, 678, and 906 cm^{-1} are attributed to vibrations of the Si-O bond in kaolinite [6]; quartz is indicated by bands at 1000 cm^{-1} and 1023 cm^{-1}; the frequency 3623 cm^{-1} is attributable to micaceous phases (illite) [6], and the band at 3701 cm^{-1} is due to the vibration of the Al-OH bond in kaolinite [7]. These results corroborate those of XRD.

2.4.3. Differential Thermal Analysis and Thermogravimetric Analysis (DTA/TGA)

The device used was a Linseis L62 DTA. It allowed us to work within a temperature range of 25˚C to 1250˚C. The heating rate we adopted was 10˚C/min. The reference sample was alumina. And in TGA the sample, placed in an alumina capsule suspended from the beam of a thermobalance, is located in a temperature-controlled chamber. The balance's equilibrium is maintained by an electromagnetic compensation system. The mass variation, determined by the rebalancing system, is recorded as a function of the temperature increase.

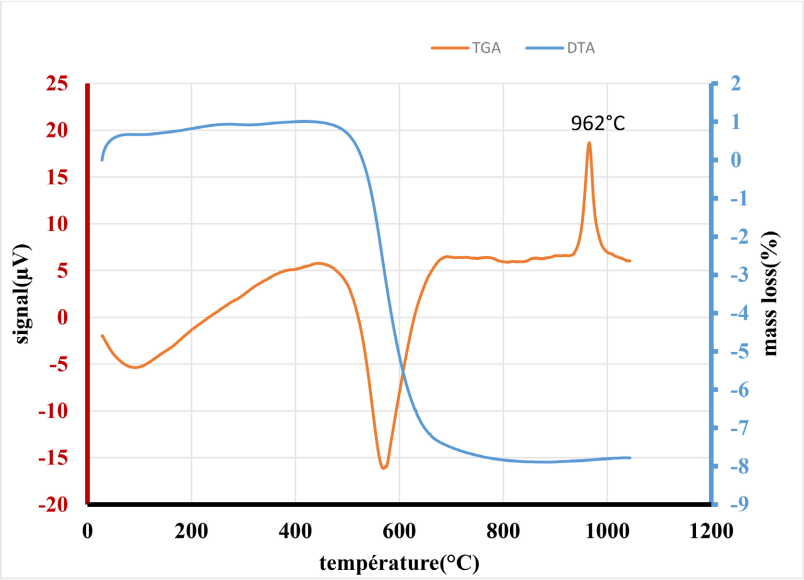

Figure 6. TGA and DTA thermograms of the Oualle clay.

Differential thermal analysis (DTA) and thermogravimetric analysis (TGA) were performed simultaneously. The DTA/TGA thermogram (**Figure 6**) shows:

- a first endothermic peak around 86˚C corresponding to the release of hygroscopic water.

- a second, very intense endothermic peak around 576˚C associated with a mass loss of 8.6%. This corresponds to the dehydroxylation of kaolinite and illite and

the allotropic transformation of α-quartz to β-quartz.

- an exothermic peak observed around 962˚C, which corresponds to the structural reorganization of metakaolinite to produce the more stable mullite (via a spinel phase) and amorphous silica [8]. The DTA/TGA results are consistent with the XRD and IR results.

2.4.4. Dilatometric Analysis

Dilatometric measurements were performed on an Adamel DI24 type dilatometer. The device is equipped with a resistance furnace. It allows investigations to be carried out in a temperature range from ambient to 1400˚C. The measurement chain consists of an alumina plunger held in contact with the sample by a spring, and an inductive displacement sensor, which measures the change in length during the test.

The dilatometric curve (**Figure 7**) initially shows expansion up to 535˚C. This is explained by the thermal expansion of the clay particles due to sintering.

A first pronounced shrinkage is observed between 535˚C and 631˚C. This relatively wide shrinkage is due to the simultaneous transformation of kaolinite, illite, and α-quartz into β-quartz; the transformation of kaolinite corresponds to its dehydroxylation into metakaolinite. The second shrinkage, between 927˚C and 978˚C, reflects the structural reorganization of metakaolinite into mullite. The shrinkage is more pronounced between 1176˚C and 1200˚C, corresponding to the densification of the material. The break at 568˚C on the cooling curve corresponds to the allotropic transformation of β-quartz into α-quartz.

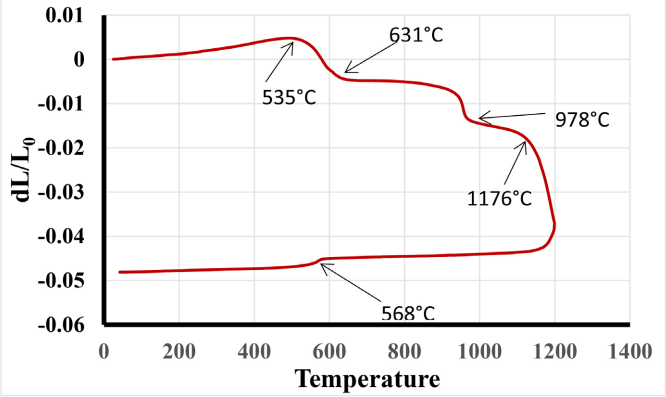

Figure 7. Dilatometric curve of the Ouallé clay.

2.4.5. Mineralogical Summary

From the results of the elemental chemical analysis and mineralogical characterization, the identified mineral phases can be quantified using the relationship proposed by Moutou *et al.* [9].

$$T(a) = \sum M_i P_i(a) \qquad \text{(Relation 3)}$$

where T (a): percentage of constituent oxide of element "a"; Mi percentage of mineral "i" and Pi (a) percentage of oxide of "a" in "i" [6].

Table 8 represents the identified mineral species along with their ideal formula and corresponding molar mass.

Table 8. Mineral species used for calculating clay phases.

Mineral species	Composition	Molar mass (g/mol)
Illite	$(K, H_3O)Al_2Si_3AlO_{10}(OH)_2$	814
Kaolinite	$Al_2(Si_2O_5)(OH)_4$	258
Quartz	SiO_2	60
Goethite	FeO(OH)	89

The various results are obtained based on the following considerations:

- K_2O is attributed solely to illite,
- Al_2O_3 is attributed to illite and kaolinite,
- SiO_2 is attributed to kaolinite, illite, and quartz,
- Fe_2O_3 is attributed to goethite.

$$\%illite = \frac{\%K2O \times 814}{94},$$

$$\%kaolinite = \frac{\%Al2O3 - \%Illite \times \frac{102 \times 3}{814}}{102} \times 258,$$

$$\%quartz = \%SiO_2 - \%kaolinite \times \frac{60 \times 2}{258} - \%Illite \frac{60 \times 6}{814},$$

$$\%goethite = \frac{\%Fe2O3}{160} \times 89.$$

With a molar mass of 102 g/mol for alumina (Al_2O_3), 60 g/mol for silica (SiO_2), 94 g/mol for potassium oxide, and 160 g/mol for iron oxide (Fe_2O_3), the mineral composition is as follows:

The results of the mineralogical analysis are recorded in Table 9. These results show that the sample is rich in kaolinite and quartz, but also contains illite and some goethii balance that indicates the presence of some additional trace clay minerals. The mineralogy of the Ouallé clay is typical of the raw materials used in red clay floor tiles and fired bricks.

Table 9. Mineralogical summary.

Phases	kaolinite	quartz	illite	goethite	balance	total
%	65	19	9	3	4	100

3. Thermomechanical Characterization of Baked Test Specimens

3.1. Formulation

The test specimen formulation was carried out at the Céramix laboratory of the

Hage Group. The sample was finely ground to a particle size of less than 100 µm before being moistened with 4 to 5% water. 250 grams of the moistened powder was used each time to prepare cylindrical 5cm in diameter, 10cm high test specimens by pressing them at a pressure of 15 MPa using a GRASEBY SPECAC press. The resulting specimens were dried at 60˚C for 24 hours before being fired at high temperature in the field of ceramics 1150˚C, 1200˚C, and 1250˚C which allows the earth to vitrify (become waterproof and very resistant) for 2 hours. The heating rate was 2˚C/min. three test tubes per chosen temperature (**Figure 8**) were then characterized for their density, water absorption, open porosity, shrinkage, and mechanical strength. The first three characteristics (density, water absorption and open porosity) are determined by the vacuum immersion method according to ISO 10545-3 [10].

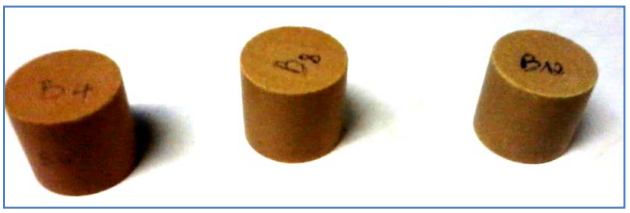

Figure 8. Test tube samples after baking.

3.2. Mass Loss - Shrinkage

The mass loss and shrinkage of the specimens during sintering are shown in **Figure 9**. Mass loss increases with temperature. This mass loss, also known as loss on ignition, is due to the release of volatile compounds and the transformation of certain mineral compounds. The higher the temperature, the closer the phase transformation temperature is reached.

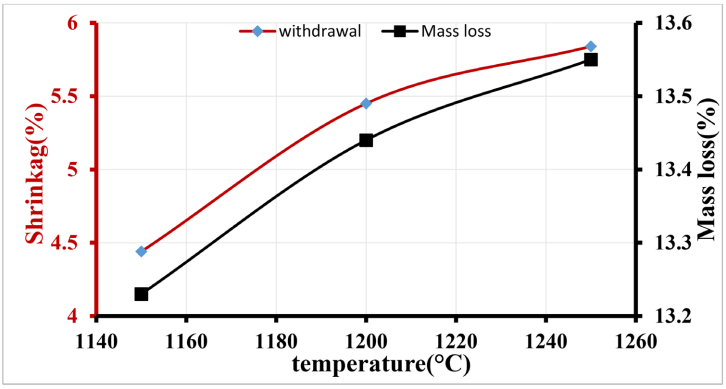

Figure 9. Variation of linear shrinkage and mass loss as a function of temperature.

Shrinkage also increases with temperature. This increase in shrinkage is due to microstructural changes in the different phases. This shrinkage is due to material consolidation. This consolidation gives the finished products better mechanical properties [11]. Shrinkage values between 4 and 6% are very desirable for use in

ceramics [12]. They indicate acceptable material consolidation.

The various shrinkages and mass losses increase with temperature in a practically similar manner. Consolidation is therefore the result of thermal phase transformation on the one hand and material densification on the other.

3.3. Porosity - Apparent Density

The evolution of porosity and apparen density as a function of temperature is shown in Figure 10. The various results corroborate those of shrinkage. The higher the firing temperature, the greater the shrinkage and the better the consolidation of the material. This consolidation occurs through the closure of existing pores, hence the decrease in porosity. Porosity is minimal at a maximum temperature [13].

Open porosity is determined by the vacuum water impregnation method. It is calculated using Equation 1:

$$P_o = \frac{P_h - P_s}{P_h - P_i} \times 100 \quad (1)$$

P_o is the open porosity;

P_s is the weight of the dry sample;

P_h is the weight of the water-filled sample;

P_i is the buoyant force exerted on the impregnated sample when it is in water.

However, despite the high firing temperatures, the porosity of the specimens remains high. It is slightly higher than the maximum value for terracotta, which is 30%.

Density varies with temperature (Figure 10). It is a function of the specific gravity ρ, determined by the ratio: ρ = m/V. As the temperature increases, shrinkage increases, therefore the volume decreases and the specific gravity increases; this leads to an increase in density.

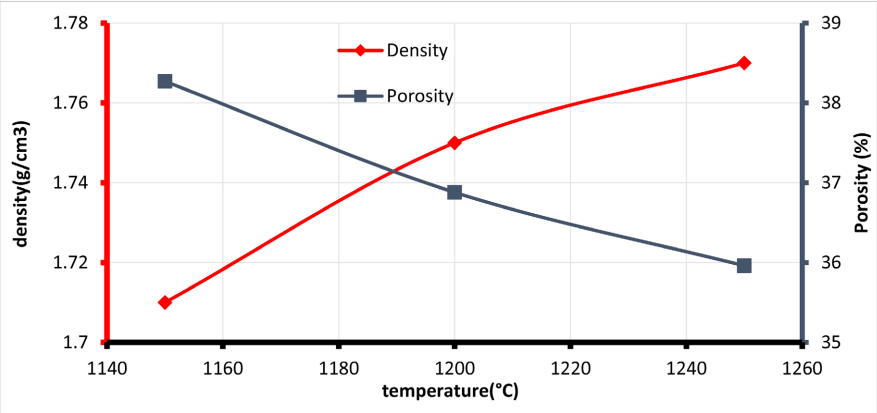

Figure 10. Evolution of porosity and density as a function of temperature.

3.4. Compressive Strength

The evolution of the compressive strength of the different grades as a function of

temperature is shown in Figure 11. Three test tubes were tested. We observe that the strength increases with temperature up to a maximum value at 1200˚C, after which the strength decreases considerably. A better consolidation of the material is observed around 1200˚C with a modulus of 16.80 MPa, a strength that corresponds to that of earthenware according to Bartusch *et al.* 2009 [14]. This is slightly lower than the minimum value for terracotta, which is 20 MPa.

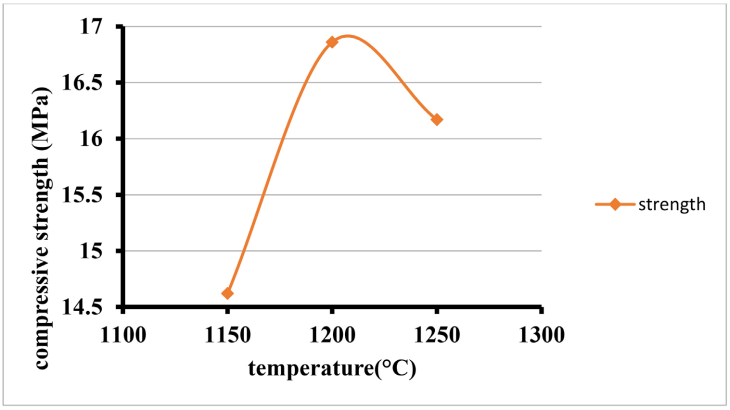

Figure 11. Evolution of resistance as a function of temperature.

4. General Conclusion

The present work focused on the characterization of the Ouallé clay deposit with a view to its valorization in ceramic applications. Several characterization techniques were combined for its analysis, followed by technological tests on specimens prepared from Ouallé clay.

Several conclusions can be drawn from the characterization of Ouallé clay:

1. Ouallé clay is mainly composed of three granular families (d_{10}, d_{50} and d_{90}) and exhibits moderate plasticity;
2. Its chemical composition represents a good balance of temper, flux, and coloring agents and corresponds to the typical composition of red-body floor tiles and fired bricks;
3. From a mineralogical point of view, it consists of 65% kaolinite, 19% quartz, 9% illite, and 3% goethite.

Ouallé clay is therefore a typical ceramic mixture, containing plasticizers, fluxes, tempers, and coloring agents. It is thus suitable for use as a base raw material in ceramic production.

Based on the technological tests, the following conclusions can be drawn:

1. The linear shrinkage, ranging between 4 and 6%, is sufficient to ensure material consolidation; according to F. Andreola *et al.* 2016 [12].
2. Porosity remains high even at elevated firing temperatures; however, it is comparable to that of faience; This corroborates Rhee's 1975 result.
3. The maximum mechanical strength (16.8 MPa) obtained at 1200˚C is close to that of fired clay products (20 MPa) and corresponds to that of faience (17 MPa).

In summary, Ouallé clay can be used as a basic raw material for the production of faience and fired clay products. However, additives are required in order to reduce the firing temperature and to improve the mechanical strength of the products. Future studies will therefore focus on proposing ceramic body formulations based on Ouallé clay using talc and feldspar as additives.

Conflicts of Interest

The authors declare no conflicts of interest regarding the publication of this paper.

References

[1] Lindsay, B. (2022) The Mineral Fraction of Soil. Pearson Education.

[2] El Yakoubi, N., Aberkan, M. and Ouadia, M. (2006) Potentialité d'utilisation d'argiles marocaines de Jbel Kharrou dans l'industrie céramique. *Comptes Rendus. Géoscience*, **338**, 693-702. https://doi.org/10.1016/j.crte.2006.03.017

[3] Sadik, C., El Amrani, I. and Albizane, A. (2012) Influence de la nature chimique et minéralogique des argiles et du processus de fabrication sur la qualité des carreaux céramiques. *MATEC Web of Conferences*, **2**, Article ID: 01016. https://doi.org/10.1051/matecconf/20120201016

[4] Aras, A. (2004) The Change of Phase Composition in Kaolinite- and Illite-Rich Clay-Based Ceramic Bodies. *Applied Clay Science*, **24**, 257-269. https://doi.org/10.1016/j.clay.2003.08.012

[5] Bensalem, H., Aadjour, M., El Hadi, H. and Saber, N. (2014) Evaluation of the Industrial Quality of Fibrous Clays from Bled Rmel, Gharb Basin, Morocco. *European Scientific Journal*, **10**, No. 2.

[6] Lanson, B., Beaufort, D., *et al.* (1996) Illitization of Diagenetic Kaolinite-To-Dickite Conversion Series: Late-Stage Diagenesis of the Lower Permian Rotliegend Sandstone Reservoir, Offshore of the Netherlands. *SEPM Journal of Sedimentary Research*, **66**, 501-518. https://doi.org/10.1306/d4268392-2b26-11d7-8648000102c1865d

[7] Ait Said, A., Bey, K., Hadriche, I. and Bradai, C. (2022) Comportement mécanique en fatigue d'un composite sandwich à âme en nids d'abeilles en flexion 3 points. https://dspace.univ-annaba.dz//handle/123456789/3411

[8] Sigg, J. (1991) Terracotta Products. Septima.

[9] Moutou, J.M., Mbedi, R., Elimbi, A., Njopwouo, D., Yvon, J., *et al.* (2012) Mineralogy and Thermal Behaviour of the Kaolinitic Clay of Loutété (Congo-Brazzaville). *Research Journal of Environmental and Earth Sciences*, **4**, 320. https://hal.science/hal-02505729v1

[10] Ndzana, E.J.A., Njoya, D., Elimbi, A., Ranaivoarivo, G.V., Lecomte-Nana, G., Nzeukou, A.N., *et al.* (2019) Cocoa Cortex Ashes as Fluxing Additive for Vitrified Ceramic Making from Alluvial Clay. *Journal of Materials Science and Chemical Engineering*, **7**, 24-39. https://doi.org/10.4236/msce.2019.710003

[11] Wu, Y., German, R.M., Blaine, D., Marx, B. and Schlaefer, C. (2002) Effects of Residual Carbon Content on Sintering Shrinkage, Microstructure and Mechanical Properties of Injection Molded 17-4 PH Stainless Steel. *Journal of Materials Science*, **37**, 3573-3583. https://doi.org/10.1023/a:1016532418920

[12] Andreola, F., Barbieri, L., Lancellotti, I., Leonelli, C. and Manfredini, T. (2016) Recycling of Industrial Wastes in Ceramic Manufacturing: State of Art and Glass Case Studies. *Ceramics International*, **42**, 13333-13338.

https://doi.org/10.1016/j.ceramint.2016.05.205

[13] Rhee, S.K. (1975) Porosity—Thermal Conductivity Correlations for Ceramic Materials. *Materials Science and Engineering*, **20**, 89-93. https://doi.org/10.1016/0025-5416(75)90134-2

[14] Bartusch, R. and Händle, F. (2009) Laminations in Extrusion. In: Händle, F., Ed., *Extrusion in Ceramics*, Springer, 187-210. https://doi.org/10.1007/978-3-540-27102-4_10